

A Multi-Messenger Search for the Supermassive Black Hole Binary in 3C 66B with the Parkes Pulsar Timing Array

JACOB CARDINAL TREMBLAY,^{1,2} BORIS GONCHAROV,^{1,2} RUTGER VAN HAASTEREN,^{1,2} N. D. RAMESH BHAT,³
ZU-CHENG CHEN,^{4,5} VALENTINA DI MARCO,^{6,7,8} SATORU IGUCHI,⁹ AGASTYA KAPUR,^{10,8} WENHUA LING,⁸
RAMI MANDOW,^{10,8} SAURAV MISHRA,^{11,7,8} DANIEL J. REARDON,^{11,7} RYAN M. SHANNON,^{11,7} HIROSHI SUDOU,¹²
JINGBO WANG,¹³ SHI-YI ZHAO,^{14,15} XING-JIANG ZHU,^{15,16} AND ANDREW ZIC^{8,7}

¹Max Planck Institute for Gravitational Physics (Albert Einstein Institute), 30167 Hannover, Germany

²Leibniz Universität Hannover, 30167 Hannover, Germany

³International Centre for Radio Astronomy Research, Curtin University, Bentley, WA 6102, Australia

⁴Department of Physics and Synergetic Innovation Center for Quantum Effects and Applications, Hunan Normal University, Changsha, Hunan 410081, China

⁵Institute of Interdisciplinary Studies, Hunan Normal University, Changsha, Hunan 410081, China

⁶School of Physics and Astronomy, Monash University, Clayton VIC 3800, Australia

⁷ARC Centre for Excellence for Gravitational Wave Discovery (OzGrav)

⁸Australia Telescope National Facility, CSIRO, Space and Astronomy, PO Box 76, Epping, 1710, NSW, Australia

⁹National Astronomical Observatory of Japan, 2-2-1 Osawa, Mitaka, Tokyo 181-8588, Japan

¹⁰Department of Mathematics and Physical Sciences, Macquarie University, NSW 2109, Australia

¹¹Centre for Astrophysics and Supercomputing, Swinburne University of Technology, Hawthorn, VIC, 3122, Australia

¹²National Institute of Technology, Sendai College, 48 Nodayama, Medeshima-Shiote, Natori, Miyagi 981-1239, Japan

¹³Institute of Optoelectronic Technology, Lishui University, Lishui 323000, China

¹⁴School of Physics and Astronomy, Beijing Normal University, Beijing 100875, China

¹⁵Department of Physics, Faculty of Arts and Sciences, Beijing Normal University, Zhuhai 519087, China

¹⁶Institute for Frontier in Astronomy and Astrophysics, Beijing Normal University, Beijing 102206, China

ABSTRACT

A sub-parsec supermassive black hole binary at the center of the galaxy 3C 66B is a promising candidate for continuous gravitational wave searches with Pulsar Timing Arrays. In this work, we search for such a signal in the third data release of the Parkes Pulsar Timing Array. Matching our priors to estimates of binary parameters from electromagnetic observations, we find log Bayes factor $\ln \mathcal{B} = 0.22$, highlighting that the source can be neither confirmed nor ruled out. We place upper limits at 95% credibility on the chirp mass $\mathcal{M} < 6.05 \times 10^8 M_{\odot}$, and on the characteristic strain amplitude $\log_{10}(h_0) < -14.44$. This partially rules out the parameter space suggested by electromagnetic observations of 3C 66B. We also independently reproduce the calculation of the chirp mass with the 3-mm flux monitor data from the unresolved core of 3C 66B. Based on this, we outline a new methodology for constructing a joint likelihood of electromagnetic and gravitational-wave data from supermassive black hole binaries. Finally, we suggest that firmly established SMBHB candidates may be treated as standard sirens for complementary constraints on the universe expansion rate. With this, we obtain constraints on the Hubble constant with 3C 66B.

Keywords: gravitational waves — pulsars: general — methods: data analysis

1. INTRODUCTION

Pulsar Timing Arrays (PTAs) are experiments for long-term monitoring of millisecond pulsar pulse arrival

times with the primary goal of detecting nanohertz-frequency gravitational waves. Recent PTA data show evidence for the nanohertz-frequency gravitational wave background (GWB, Goncharov et al. 2021a; Arzoumanian et al. 2020a; Chen et al. 2021; Antoniadis et al. 2022; Agazie et al. 2023a; EPTA Collaboration et al. 2023; Reardon et al. 2023). The background origin is consistent with the superposition of adiabatically

jacob.cardinaltremblay@aei.mpg.de

boris.goncharov@me.com

inspiraling supermassive black hole binaries (SMBHBs) (Goncharov et al. 2024). Provided confident detection of the background, the detection of a continuous gravitational wave (CGW) from an individual SMBHB is the next milestone for PTAs. Such an observation would decisively resolve the final parsec problem, which represents difficulties in modeling the evolution of SMBHBs to sub-parsec separations. When the host galaxy of CGW is known, the detection unlocks multi-messenger astronomy and cosmology with PTAs.

One of the most promising sources of CGWs is the supermassive black hole binary candidate in the center of galaxy 3C 66B. By using long-baseline interferometry, Sudou et al. (2003) found evidence for elliptical binary orbital motion in this radio galaxy’s core and inferred a gravitational wave (GW) frequency of $f_{\text{GW}} = 60.4 \pm 1.73$ nHz. Further observations by Iguchi et al. (2010) found that the binary has a chirp mass $\mathcal{M} = 7.9^{+3.8}_{-4.5} \times 10^8 M_{\odot}$. Galaxy 3C 66B is located at a redshift $z = 0.02126$ (van den Bosch et al. 2015), which corresponds to the luminosity distance $D_L = 94.17^{+0.20}_{-0.20}$ Mpc (Planck Collaboration et al. 2020). Based on the above, the expected strain amplitude h_0 of a CGW at 3C 66B is $7.3^{+6.8}_{-5.8} \times 10^{-15}$. This is the highest known strain amplitude of CGW sources in the PTA frequency band, and is within reach for PTA experiments. The summary of the expected properties of the SMBHB at 3C 66B is shown in Table 1. Because the properties in the table are inferred from electromagnetic (EM) observations, we will also refer to this model of the SMBHB at 3C 66B as the EM model.

Table 1. Summary of properties of the SMBHB candidate at 3C 66B.

	Value	Reference
\mathcal{M}	$7.9^{+3.8}_{-4.5} \times 10^8 M_{\odot}$	Iguchi et al. (2010)
f_{GW}	60.4 ± 1.73 nHz	Sudou et al. (2003)
D_L	94.17 ± 0.20 Mpc	van den Bosch et al. (2015)
R.A.	02h 23m 11.4110s	Hunt et al. (2021)
Decl.	+42d 59m 31.385s	Hunt et al. (2021)
h_0	$7.3^{+6.8}_{-5.8} \times 10^{-15}$	Iguchi et al. (2010)

It is worth noting that Iguchi et al. (2010) revised the chirp mass of the SMBHB in 3C 66B inferred in the earlier work of Sudou et al. (2003). The initial model of the SMBHB at the center of 3C 66B proposed by Sudou et al. (2003) suggested a very high chirp mass of $1.3 \times 10^{10} M_{\odot}$. Jenet et al. (2004) has ruled out this model based on seven years of timing from

PSR B1855+09 (Kaspi et al. 1994). Assuming a circular SMBHB at 3C 66B, they placed an upper limit of $7 \times 10^9 M_{\odot}$ on its chirp mass. This upper limit does not exclude the model by Iguchi et al. (2010), which motivates further studies.

Following the revision of the chirp mass of the SMBHB candidate by Iguchi et al. (2010), a number of searches for a CGW from 3C 66B with PTAs have been performed. The authors of Arzoumanian et al. (2020b) performed a search for an SMBHB in a circular orbit with the 11-year dataset of the North American Nanohertz Observatory for Gravitational Waves (NANOGrav). An upper limit on the chirp mass of $1.65 \times 10^9 M_{\odot}$ was placed. A subsequent search was then performed for both circular and eccentric SMBHBs using the NANOGrav 12.5-year dataset. The search for a circular binary (Arzoumanian et al. 2023) constrained the mass to $1.41 \times 10^9 M_{\odot}$. The search, which included eccentricity in the SMBHB system (Agazie et al. 2024), placed their tightest constraints on the upper limit of chirp mass as $1.81 \times 10^9 M_{\odot}$. The results from the 12.5-year NANOGrav dataset are all still compatible with the Iguchi et al. (2010) model, yet claim no detection, which motivates further searches for the source in pulsar timing array datasets. With NANOGrav 15-year data, the limit on the chirp mass at 95% credibility is $9.54 \times 10^8 M_{\odot}$ (Agarwal et al. 2025).

In this work, we perform a search for CGW from an SMBHB in a circular orbit at 3C 66B using the third data release (DR3) of the Parkes Pulsar Timing Array (PPTA) (Zic et al. 2023). It is the first targeted search for 3C 66B with the PPTA data. We expect the search based on this data to provide better constraints on CGW from 3C 66B, thanks to an increased time span exceeding 18 years in 13 pulsars. The targeting is performed by setting the sky position as a fixed parameter, as well as setting priors for other parameters based on electromagnetic observations summarized in Table 1. We employ both Bayesian and frequentist methods to calculate the significance of the hypothesis that an SMBHB with sub-parsec separation resides in 3C 66B. Finally, we illustrate current capabilities of cosmology with PTAs by constraining the Hubble constant based on the premise that an SMBHB exists at 3C 66B.

The rest of the paper is organized as follows. In Section 2, we introduce the dataset from the third data release of the PPTA. In Section 3, we introduce the signal model, the Bayesian analysis methodology, and our noise models. In Section 4, we present our results and discuss the model selection, upper limits on the chirp mass, upper limits on the characteristic strain amplitude, upper limits as a function of CGW frequency, the

frequentist analysis results, and how targeted searches in PTAs can be used for cosmology experiments. In Section 5 we present our conclusions.

2. DATA

The Parkes Pulsar Timing Array dataset (Zic et al. 2023) is based on monitoring of $N_{\text{psr}} = 32$ millisecond radio pulsars. The total observing span of PPTA DR3 is $T_{\text{obs}} = 18$ years. The first observations took place on February 6, 2004, and the last observations took place on March 8, 2022. The observations were conducted using the 64-m Parkes ‘Murriyang’ radio telescope in Australia, and observations were taken for each pulsar approximately every three weeks. The most recent 3 years of observations in DR3 are carried out using the ultra-wide bandwidth, low-frequency receiver (UWL, Hobbs et al. 2020). In this work, only the data from 31 pulsars are used. PSR J1741+1351 is excluded from the analysis due to the fact that it was only added to the PPTA observations after the commissioning of the UWL and was only observed with low priority. With only 16 observations, this pulsar is not sensitive to any CGW signal and will therefore not contribute to the results.

As with any PTA data, PPTA DR3 is a set of pulse arrival time observations, including observation details such as radio frequency and backend-receiver information, as well as the pulsar ephemeris, known as the timing model. A timing model predicts pulse arrival times based on the pulsar-specific spin, astrometry, properties of the interstellar plasma along the line of sight, and the binary parameters of the pulsar when applicable. We use the DE440 ephemeris (Park et al. 2021) to obtain pulse arrival times in an inertial frame centered at the Solar System Barycenter (SSB).

Additionally, we follow Iguchi et al. (2010) by employing the same millimeter-wavelength flux variation data for 3C 66B. There are two components of this data. The first component of the data is collected at 93.7 GHz using the Nobeyama Millimeter Array (NoMA) of the National Astronomical Observatory of Japan (NAOJ). The second component of the data is collected at 86.2 GHz using the Plateau de Bure Interferometer (PdBI) of the Institut de Radioastronomie Millimétrique (IRAM).

3. METHODOLOGY

3.1. Signal Model

We use the CGW signal model for non-spinning SMBHBs in circular¹ orbits at zeroth post-Newtonian order described in (Aggarwal et al. 2019; Arzoumanian et al.

2020b, 2023). More details of the model are provided in Appendix A. The CGW model for metric perturbations at SSB (the Earth term) is based on 8 parameters:

$$\{\theta, \phi, f_{\text{GW}}, \Phi_0, \psi, i, \mathcal{M}, (D_{\text{L}} \wedge h_0)\} \quad (1)$$

Where (θ, ϕ) is the sky position, f_{GW} is the gravitational wave frequency, Φ_0 is the orbital phase, ψ is the gravitational wave polarization angle, i is the binary inclination angle, \mathcal{M} is the chirp mass, D_{L} is the luminosity distance and h_0 is the gravitational strain amplitude. At zeroth post-Newtonian order, we compute the amplitude as

$$h_0 = \frac{2(G\mathcal{M})^{5/3}(\pi f_{\text{GW}})^{2/3}}{D_{\text{L}}c^4}, \quad (2)$$

unless it is provided as a free parameter (hence, $D_{\text{L}} \wedge h_0$). The full CGW model is based on metric perturbations at both the SSB and each pulsar (pulsar terms). This requires additional $2N_{\text{psr}}$ parameters $\{L_i, \Phi_i\}$, $i = (1, N_{\text{psr}})$. They are the pulsar distance and the orbital phase at the pulsar, respectively. We provide more information on pulsar distance in Appendix C. Searching only for the Earth term is sufficient for detection and upper limits, whereas including the pulsar term enhances the search sensitivity and remains important for parameter estimation when the signal is detected.

We model the evolution of CGW frequency on the timescales of light travel time between pulsars and Earth. However, for simplicity, we neglect frequency evolution on the timescale of PPTA DR3. This approach is referred to as the stationary phase approximation. To demonstrate the validity of this approach, we employ the equation for the evolution of CGW frequency as a function of time at zeroth post-Newtonian order from (Abbott et al. 2017a),

$$f_{\text{GW}}^{-8/3}(t) = \frac{(8\pi)^{8/3}}{5} \left(\frac{G\mathcal{M}}{c^3} \right)^{5/3} (t - t_c), \quad (3)$$

where f_{GW} is the gravitational wave frequency, G is Newton’s constant, c is the speed of light, and t_c is the time of coalescence. We present the expected frequency evolution of 3C 66B at SSB in Figure 1. Based on the EM model for 3C 66B, a circular SMBHB is only expected to evolve by about 0.04 nHz/year. In the 20 years since the initial frequency was determined by Sudou et al. (2003), the frequency may have increased by 0.86 nHz. This width does not exceed the frequency resolution of PPTA DR3 of $T_{\text{obs}}^{-1} = 1.75$ nHz. Therefore, according to the model provided by Sudou et al. (2003), the stationary phase approximation is sufficient for our analysis.

¹ Iguchi et al. (2010) point out that 3C 66B may be in a circular orbit.

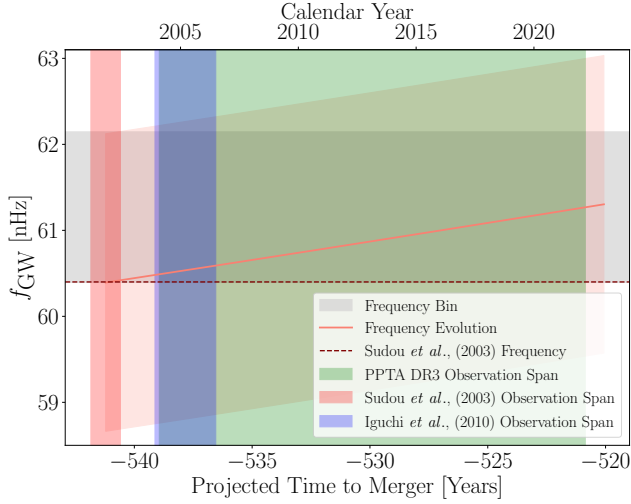


Figure 1. The evolution of the CGW frequency of 3C 66B at the SSB and the associated uncertainty from Sudou *et al.* (2003) is shown by the pink diagonal line. The dashed red line and the shaded red region show the frequency inferred by and their measurement uncertainty, respectively. The vertical red band represents the observing time frame of Sudou *et al.* (2003). The blue shaded region represents the observing time frame of Iguchi *et al.* (2010). The green shaded region represents the observing time frame of the PPTA DR3 dataset. The gray shaded region represents one frequency bin in PPTA DR3 based on T_{obs}^{-1} .

3.2. Bayesian inference

We perform parameter estimation and model selection by computing posteriors, $\mathcal{P}(\theta|\delta t) = \mathcal{Z}^{-1} \mathcal{L}(\delta t|\theta) \pi(\theta)$, where $\mathcal{L}(\delta t|\theta)$ is the likelihood of data time series vector δt given a vector of model parameters θ for signals and noise, and $\pi(\theta)$ is the prior. The constant \mathcal{Z} is the integral of the numerator over θ . It is also referred to as the evidence or the fully marginalized likelihood. We neglect \mathcal{Z} in our parameter estimation and obtain posterior samples using parallel-tempered Markov-Chain Monte-Carlo (Ellis & van Haasteren 2019). The model selection follows from computing Bayes factors, $\mathcal{B} = \mathcal{Z}/\mathcal{Z}_{\emptyset}$, where \mathcal{Z}_{\emptyset} is the evidence of the noise model and \mathcal{Z} is the evidence of the signal model, which includes both the noise and the CGW. Instead of computing \mathcal{Z} separately for the two models, we compute the Bayes factor directly using the product-space sampling method (Hee *et al.* 2016).

We use the multivariate Gaussian likelihood (van Haasteren *et al.* 2009)

$$\mathcal{L}(\delta t|\theta) = \frac{\exp\left(-\frac{1}{2}(\delta t - \mu)^T C^{-1}(\delta t - \mu)\right)}{\sqrt{\det(2\pi C)}}, \quad (4)$$

where vector μ , a function of θ , represents a prediction of deterministic contributions to pulse arrival times δt , which includes a CGW model, as well as deterministic noise transients such as exponential dips in pulse arrival times (Goncharov *et al.* 2021b). The form of our covariance matrix C and the methods for computing it are described in detail in Arzoumanian *et al.* (2016). In short, $C = N + T^T B^{-1} T$, where diagonal matrix N represents temporally uncorrelated “white” noise, T is the design matrix for reduced-rank modeling (Lentati *et al.* 2013), and B is the covariance matrix of reduced-rank coefficients b . The likelihood is marginalised over b , which determines the time series realisation Tb . Thus, the design matrix T is a mapping from the parameter space b to the time series. It is made up of three blocks. Block M maps timing model parameters to the time series. Block F maps Fourier sine and cosine amplitudes of time-correlated “red” noise to the time series. Block U maps delays in arrival times at different observing epochs due to pulse jitter to all arrival times. Coefficients b are assumed to be samples from the zero-mean Gaussian distribution described by the covariance matrix B . For the coefficients of the pulsar timing model, we assume an uninformative prior with a standard deviation of 10^{40} in respective units, which is much greater than the typical coefficient value.

3.3. Noise Model

Noise modeling in PTAs is crucial for correct astrophysical interpretability of the gravitational wave searches (Goncharov *et al.* 2024). Broadly, modeled PTA noise is categorized into temporally-uncorrelated (white) noise, temporally-correlated (red) noise with the power spectral density modeled as a power law, as well as noise transients. We use the noise model from Reid *et al.* (2023). In addition to this, we model the contribution of the common-spectrum noise process associated with the GWB (Goncharov *et al.* 2022). It is shown in Zhao *et al.* (2025) that not modeling this process leads to false positives. Agazie *et al.* (2023b) suggests that further modeling of the Hellings & Downs (1983) correlations may be necessary for the data where they are evident. This may be required for future CGW searches with the PPTA data. Furthermore, we impose a minimum allowed value of the red noise power spectral density of $T_{\text{obs}} \times 10^{-20} [\text{s}^3]$, which is well below the noise in PPTA DR3. This is done to avoid numerical errors in the likelihood.

3.4. Analysis of the 3-mm data

To perform an re-analysis of the 3C 66B 3-mm flux measurements from Iguchi *et al.* (2010), we employ the

univariate Gaussian likelihood, $\mathcal{L}(\mathbf{S}|\boldsymbol{\theta}_{\text{EM}})$, where \mathbf{S} is a vector of flux measurements in units mJy. The general form is the same as Equation 4, except that the covariance matrix is diagonal with elements $\sigma_{\text{EM}}^2 = \sigma_S^2 e_f^2 + e_q^2$. Here, σ_S is the flux measurement uncertainty. White noise parameters (e_f, e_q) are the error factor and the error added in quadrature. The analogue of $\boldsymbol{\mu}$ from Equation 4 for the EM data is the sine-cubic function from Iguchi et al. (2010):

$$\begin{aligned} \mathbf{S}(t) = & A_{\text{EM}} \sin(2\pi f_{\text{EM}} t + \phi_{\text{EM}}) + \\ & + a_{\text{EM}}(t - t_0)^3 + b_{\text{EM}}(t - t_0)^2 + \\ & + c_{\text{EM}}(t - t_0) + d_{\text{EM}} \end{aligned} \quad (5)$$

In total, $\boldsymbol{\theta}_{\text{EM}}$ is a set of parameters (e_f, e_q, A_{EM} [mJy], f_{EM} [Hz], ϕ_{EM} , t_0 [s], a_{EM} [mJy/s³], b_{EM} [mJy/s²], c_{EM} [mJy/s], d_{EM} [mJy]).

The chirp mass is calculated from $\boldsymbol{\theta}_{\text{EM}}$ and Equation 5 as follows. Iguchi et al. (2010) suggest that the sine component is due to the Doppler boosting of the flux from the core of 3C 66B due to binary motion around the center of mass, whereas the cubic component may be responsible for the non-thermal radiation in the knots of the jet in the core. From the frequency of the sine component f_{EM} , the SMBHB orbital frequency f_k from Sudou et al. (2003), and the apparent boost in the relativistic jet β_{app} (Iguchi et al. 2010), we compute the jet outflow boost β and the inclination angle ι between the jet axis and the line of sight. The flux ratio from Doppler boosting is $\mathbf{S}_r = \max(\mathbf{S})/\min(\mathbf{S})$, where $\max(\mathbf{S}) = \bar{S} + A_{\text{EM}}$ and $\min(\mathbf{S}) = \bar{S} - A_{\text{EM}}$ are computed from the mean flux \bar{S} . From the above, assuming the power law relation between the Doppler factor and \mathbf{S}_r with a spectral index α , we calculate the SMBHB orbital radius. Considering that the jet originates from one of the black holes in a binary, but not two, and from the total mass of the binary M_{tot} , which can be computed based on the galaxy velocity dispersion relation, a chirp mass \mathcal{M} is obtained. To sum up, $\mathcal{M} = \mathcal{G}(\boldsymbol{\theta}_{\text{EM}}, \boldsymbol{\varphi})$, where $\boldsymbol{\varphi} = (f_k, \beta_{\text{app}}, M_{\text{tot}}, \alpha)$ and \mathcal{G} is a function with the aforementioned operations. For more details, please refer to Appendix B and Iguchi et al. (2010).

3.5. Multi-messenger likelihood

Here, we lay out the groundwork for the joint analysis of CGW and EM data, which may be explored in future work. Because EM and CGW data are independent, the total likelihood of these data is a product of the likelihoods: $\mathcal{L}(\boldsymbol{\delta t}, \mathbf{S}|\boldsymbol{\theta}) = \mathcal{L}(\boldsymbol{\delta t}|\boldsymbol{\theta})\mathcal{L}(\mathbf{S}|\boldsymbol{\theta}_{\text{EM}})$, where $\boldsymbol{\theta} = (\boldsymbol{\theta}_{\text{GW}}, \mathcal{M})$. Effectively, the common parameter in both the CGW and the EM model from Iguchi et al. (2010) is the chirp mass \mathcal{M} . Therefore, the posterior is $\mathcal{P}(\boldsymbol{\theta}_{\text{GW}}, \boldsymbol{\theta}_{\text{EM}}, \boldsymbol{\varphi}|\boldsymbol{\delta t}, \mathbf{S}) =$

$\mathcal{L}(\boldsymbol{\delta t}, \mathbf{S}|\boldsymbol{\theta}_{\text{GW}}, \boldsymbol{\theta}_{\text{EM}}, \boldsymbol{\varphi})\pi(\boldsymbol{\theta}_{\text{GW}})\pi(\boldsymbol{\theta}_{\text{EM}})\pi(\boldsymbol{\varphi})$. Here, we also express $\mathcal{L}(\boldsymbol{\delta t}|\boldsymbol{\theta}_{\text{GW}}, \boldsymbol{\theta}_{\text{EM}}, \boldsymbol{\varphi}) = \mathcal{L}(\boldsymbol{\delta t}|\boldsymbol{\theta}_{\text{GW}}, \mathcal{M} = \mathcal{G}(\boldsymbol{\theta}_{\text{EM}}, \boldsymbol{\varphi}))$.

4. RESULTS

4.1. Model selection

We first perform model selection by calculating the Bayesian evidence in favor of an SMBHB at 3C 66B against the null hypothesis. For this calculation, we match our prior on CGW parameters to the results of EM searches. This approach allows for precise confirmation or exclusion of the EM model. In particular, for the \log_{10} chirp mass, we use a skewed Normal prior with hyperparameters for skewness, mean, and the standard deviation which have values of $-3.08, 9.12 [\log_{10} M_{\odot}]$ and $0.42 [\log_{10} M_{\odot}]$, respectively. We found empirically that this prior has the same unequal uncertainty levels as constraints from EM data in Table 1. Similarly, we fix the luminosity distance based on the redshift of 3C 66B, assuming the Λ CDM cosmological model based on Planck Collaboration et al. (2020). We use an exponential-Normal prior for $\log_{10} f_{\text{GW}}$, with mean and variance from Table 1. We perform this calculation with only the Earth term of the CGW. Finding $\ln \mathcal{B} = 0.22$, we find no evidence for an SMBHB at 3C 66B; nevertheless, we cannot rule out the EM model. Therefore, we place limits on the parameters of a potential SMBHB at 3C 66B.

4.2. Limits on the SMBHB chirp mass at 3C 66B

We perform parameter estimation of the log-10 chirp mass. As in the previous calculation, we assume the luminosity distance as a fixed parameter based on the known redshift of 3C 66B and Planck 2018 results (Planck Collaboration et al. 2020). The difference is that now we use a broad uniform prior $\pi(\log_{10} \mathcal{M}) = \mathcal{U}(7.5, 9.5) [\log_{10} M_{\odot}]$. This provides a more EM-independent perspective consistent with the decreasing probability of finding an SMBHB towards high $\mathcal{M} > 10^9 M_{\odot}$ in nature at $z = 0$ (Hopkins et al. 2007), defined by the SMBHB mass function. We also use a more convenient prior on $\pi(\log_{10}(f_{\text{GW}})) = \mathcal{N}(-7.22, 0.01) [\log_{10} \text{Hz}]$, which is still consistent with the EM model.

The results are shown in Figure 2. When only the Earth term is modeled in our analysis, we find an upper limit of $\mathcal{M} < 8.25 \times 10^8 M_{\odot}$ at 95% credibility. When including the pulsar term, we find a more constraining limit, $\mathcal{M} < 6.05 \times 10^8 M_{\odot}$. For comparison, we show the value from the EM model from Iguchi et al. (2010), $(7.9^{+3.8}_{-4.5}) \times 10^{-8} M_{\odot}$. Our limits are not below the prediction of the EM model. Therefore, we can-

not rule it out. However, the tightest upper limit calculated rules out 53% of the uncertainty region of the EM-model. For consistency with [Arzoumanian et al. \(2023\)](#); [Agarwal et al. \(2025\)](#), we also obtain a posterior by reweighting our posteriors to a uniform prior in linear space $\pi(\mathcal{M}) = \mathcal{U}(10^{7.5}, 10^{9.5}) [M_\odot]$. While not matching astrophysical expectations for the SMBHB mass function, this presents the most conservative limits. With this prior, we report an upper limit at 95% credibility to be $\mathcal{M} < 11.06 \times 10^8 M_\odot$ for the Earth term and $\mathcal{M} < 9.55 \times 10^8 M_\odot$ when the pulsar term is included. Our limits are a factor of 2.73 lower compared to [Arzoumanian et al. \(2020b\)](#), a factor of 2.21 lower compared to [Arzoumanian et al. \(2023\)](#), and the same as in [Agarwal et al. \(2025\)](#).

We also report the result of our reanalysis of the 3-mm data from [Iguchi et al. \(2010\)](#). Following the methodology in Section 3.4, we obtain a posterior on the log-10 chirp mass of the SMBHB at 3C 66B. It is shown as the black shaded area in Figure 2. The posterior is skewed towards higher masses, consistently with the uncertainties reported in [Iguchi et al. \(2010\)](#) and presented in Table 1.

4.3. Limits on the gravitational wave strain from 3C 66B

Instead of calculating the strain amplitude h_0 of the CGW from 3C 66B based on the luminosity distance using Equation 2, we now treat it as a free parameter. This way, the distance to 3C 66B is not involved in the calculation. Similar to the chirp mass prior, we use a prior $\pi(\log_{10} h_0) = \mathcal{U}(-17.0, -12.5)$, which is more consistent with the decreasing probability of an SMBHB with a high h_0 . The other priors are as in Section 4.2. The posterior on h_0 is shown in Figure 3. With only the Earth term, we find an upper limit at 95% credibility to be $\log_{10} h_0 < -14.12$. When including the pulsar term, we find a more constraining limit, $\log_{10} h_0 < -14.44$. Using the more conservative prior, $\pi(h_0) = \mathcal{U}(10^{-17.0}, 10^{-12.5})$, we find an upper limit for the Earth term of $\log_{10} h_0 < -13.86$ and an upper limit of $\log_{10} h_0 < -14.20$ when including the pulsar term. As in Section 4.2, the range of h_0 of the EM model from [Iguchi et al. \(2010\)](#) is partially ruled out in all cases.

It is also of interest to compare the strain amplitude of a CGW signal from 3C 66B with the expectation for the GWB at the EM-predicted frequency of the binary. [Goncharov et al. \(2024\)](#) proposes a fiducial prior on the characteristic strain amplitude of the background, $h_c(f) = A(f \text{ yr})^{-2/3}$, characteristic of SMBHBs. The prior is based on black hole masses inferred

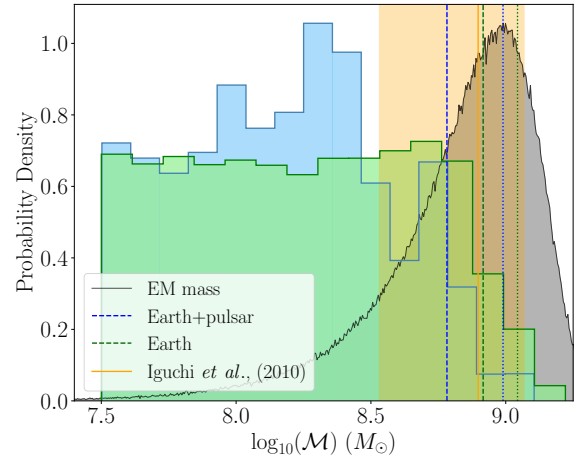


Figure 2. Observational constraints on the chirp mass \mathcal{M} of an SMBHB at 3C 66B. The histograms show a posterior for \mathcal{M} based on the analysis of PPTA DR3. The dashed lines show the respective upper limits at 95% credibility based on the astrophysically-motivated prior $\pi(\log_{10} \mathcal{M}) = \mathcal{U}(7.5, 9.5) [\log_{10} M_\odot]$. The dotted lines show the limits based on the conservative prior $\pi(\mathcal{M}) = \mathcal{U}(10^{7.5}, 10^{9.5}) [M_\odot]$. In green, we show the results of the analysis with only the Earth term of the signal modeled. In blue, we show the results based on modeling both the Earth term and the pulsar term of the CGW. The black solid line with arbitrary density normalization represents the posterior we obtain from the 3-mm data analyzed in [Iguchi et al. \(2010\)](#). The vertical orange line and the band correspond to the value and the uncertainty reported in [Iguchi et al. \(2010\)](#).

from kinematic observations and galaxy velocity dispersion. Based on this prior, we calculate $h_{0,\text{GWB}} = 2h_c/\sqrt{32/5}$, to revert the root-mean-square averaging over SMBHB inclination and polarization assumed for the background (see Equation 8 in [Burke-Spolaor et al. \(2019\)](#)). The best-fit $h_c(f = \text{yr}^{-1})$ of the GWB from the data of the European Pulsar Timing Array by [Goncharov et al. \(2024\)](#) is within 3σ interval of the prior, above the prior mean. Thus, the prior is consistent with observations.

The prior from [Goncharov et al. \(2024\)](#) marginalized over $\pi(f_{\text{CGW}})$ is shown as the solid black line in Figure 3, elucidating a connection between the EM model of the CGW candidate 3C 66B and the expected GWB. The comparison suggests the following:

- The EM model of 3C 66B corresponds to a loud source in the expected GWB.
- A fraction of the parameter space of the EM model for 3C 66B, which we have ruled out, is also not supported by the predicted GWB amplitude.

- Our limits at f_{CGW} of 3C 66B are, on average, higher than the expected GWB because we are limited by the white noise at the frequency of 3C 66B.

The value $h_{0,\text{GWB}}$ can also be interpreted as the equivalent expected CGW amplitude of the background if it is dominated by one source (3C 66B) at 3C 66B CGW frequency. This scenario is possible, given the scaling of the number of SMBHB sources contributing to the background with frequency. This may also lead to a deviation from the power-law model for $h_c(f)$ at the frequency of 3C 66B, depending on the number density of SMBHBs. It is also worth noting that [Zhu et al. \(2019\)](#) find that the EM model for 3C 66B is in tension with the observed GWB amplitude based on the expected SMBHB merger rate.

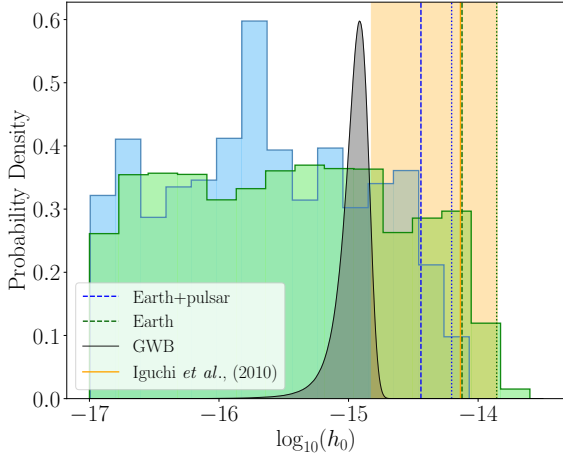


Figure 3. Observational constraints on the CGW strain amplitude, h_0 , of an SMBHB at 3C 66B. The histograms show a posterior for h_0 based on the analysis of PPTA DR3. The dashed lines show the respective upper limits at 95% credibility based on the astrophysically-motivated prior $\pi(\log_{10} h_0) = \mathcal{U}(-17.0, -12.5)$. The dotted lines show the limits based on the conservative prior $\pi(h_0) = \mathcal{U}(10^{-17.0}, 10^{-12.5})$. In green, we show the results of the analysis with only the Earth term of the signal modeled. In blue, we show the results based on modeling both the Earth term and the pulsar term of the CGW. The black solid line with arbitrary density normalization represents the theoretically expected gravitational wave background contribution at the frequency of 3C 66B. The vertical orange line and the band correspond to the value and the uncertainty reported in [Iguchi et al. \(2010\)](#).

4.4. Upper limits as a function of CGW frequency

Following [Arzoumanian et al. \(2020b\)](#), for a broader perspective on how PPTA DR3 limits on \mathcal{M} depend

on f_{GW} for any SMBHB at the position of 3C 66B, we show Figure 4. For this calculation, we use the same prior as in Section 4.2, except the prior on CGW frequency is now $\pi(\log_{10} f_{\text{GW}}) = \mathcal{U}(-9.0, -7.0)$ [\log_{10} Hz]. We also only model the Earth term of the CGW. The figure highlights that the PPTA is well-suited to target 3C 66B, as the value suggested by the EM model is at the frequency to which our targeted search is most sensitive. Consistent with Figure 2, when modeling the pulsar term and using astrophysically motivated priors, we are close to ruling out the best-fit value of the EM model. We observe the highest density of posterior samples at around $f_{\text{GW}} = \text{yr}^{-1}$, which corresponds to uncertainties associated with measuring pulsar positions. There is also a minor over-density of posterior samples at $f_{\text{GW}} = (2 \text{ yr})^{-1}$, which corresponds to uncertainties associated with measuring pulsar parallax. Given that the posterior is not uniform at these frequencies, some of the uncertainties may be systematic.

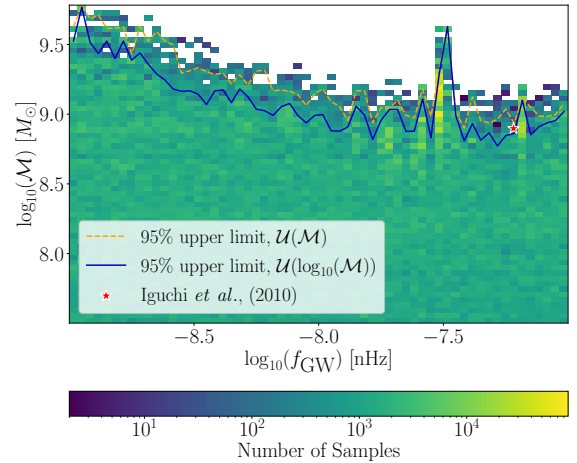


Figure 4. Posterior for the chirp mass \mathcal{M} and frequency f_{GW} of 3C 66B. The color map shows the number of posterior samples in the \mathcal{M} - f_{GW} space. The best-fit value from [Iguchi et al. \(2010\)](#) is shown as a red star. The blue solid line shows the respective upper limit at 95% credibility based on the astrophysically-motivated prior $\pi(\log_{10} \mathcal{M}) = \mathcal{U}(7.5, 10.5)$ [$\log_{10} M_{\odot}$]. The yellow dashed line shows the limits based on the conservative prior $\pi(\mathcal{M}) = \mathcal{U}(10^{7.5}, 10^{10.5})$ [M_{\odot}].

4.5. Frequentist Search

To confirm the non-detection of a CGW, we perform the frequentist targeted search based on the \mathcal{F} statistic ([Ellis et al. 2012](#)), a frequentist measure of evidence

for a CGW in our data. In particular, we chose to calculate the \mathcal{F}_e statistic, which is based on only modeling the Earth term of CGW. This statistic is a function of CGW frequency and sky position, which we set to the 3C 66B EM model values. We find the value of $\mathcal{F}_e = 4.90$, corresponding to the false alarm probability $\text{FAP} = 0.50$. Ellis et al. (2012) suggest a threshold for FAP to be 10^{-4} to claim a detection. The trials factor for our search is 1. The background distribution of the \mathcal{F}_e statistic is the chi-squared distribution with 4 degrees of freedom and is displayed in Figure 5 along with the value of the $2\mathcal{F}_e$ statistic. Based on this null distribution, we find a $p\text{-value} = 0.04$ which corresponds to about 2.1σ . Thus, the \mathcal{F}_e statistic value we find is consistent with noise.

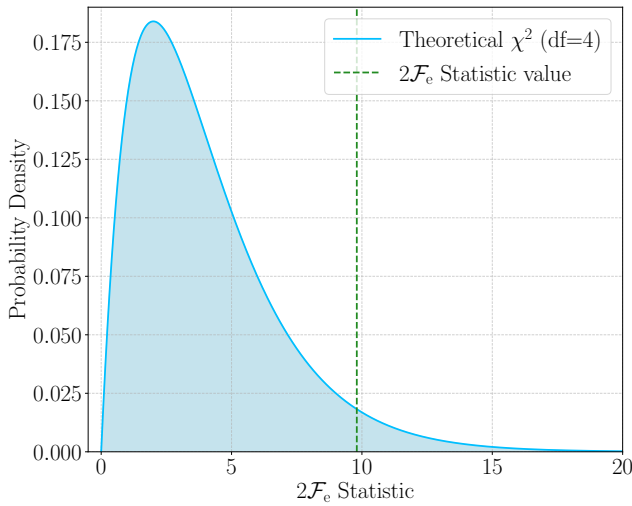


Figure 5. The background distribution of the \mathcal{F}_e statistic, which is a chi-squared distribution with 4 degrees of freedom. The green vertical dashed line is the $2\mathcal{F}_e$ statistic calculated at the frequency and sky position of 3C 66B.

4.6. Cosmology based on targeted searches with PTAs

Standard sirens are compact binaries that emit gravitational and electromagnetic (EM) radiation simultaneously, allowing for measurement of the universe’s expansion rate (Schutz 1986). Redshift of the host galaxy of a standard siren from EM information enables the determination of its recessional velocity v . Whereas the proper distance D is measured based on the gravitational wave signal. The Hubble constant, which quantifies the universe’s expansion at the present time, is

$$H_0 = \frac{v}{D}. \quad (6)$$

The primary challenge in the standard siren approach is localizing the electromagnetic (EM) counterpart of a gravitational wave. To this date, the first observed

binary neutron star inspiral, GW170817 (Abbott et al. 2017a), is the only gravitational wave signal for which an EM counterpart is established: galaxy NGC 4993. The sky position uncertainty for GW170817 is 28 deg^2 at 90% credibility. For PTAs, the sky position uncertainty for all-sky CGW searches is expected to be less precise. Moreover, the signals are not transient, which makes identification of the host galaxy even more difficult. For example, IPTA-DR3 simulations (116 pulsars, 20-year baseline) from Petrov et al. (2024) found that for an ideal case where the signal-to-noise ratio (SNR) is of $\text{SNR} = 15$, 90% credible area would range from 29 deg^2 to 241 deg^2 . However, for a realistic case, with $\text{SNR} = 8$, the 90% credible area increases from 287 deg^2 to 530 deg^2 . Petrov et al. (2024) concludes that without better CGW localization, host galaxy searches are impractical. Truant et al. (2025) have additionally simulated a 30-year SKA-PTA observation and found that out of the ≈ 35 CGW detected, only 35% have a 90% credible area $< 100 \text{ deg}^2$. They conclude that observations with an $\text{SNR} > 25$ will have fewer than 100 host galaxy candidates. Even in simulations which look at a very high SNR, such as those performed by Zhu et al. (2016), with a 15-year baseline and 30 pulsars, a strong signal with $\text{SNR} = 100$ yields a localization of $\sim 40 \text{ deg}^2$. Therefore, standard siren cosmology based on all-sky CGW searches is not feasible with currently operating PTAs.

Targeted PTA searches for SMBHB candidates eliminate the problem of finding the electromagnetic counterpart of a gravitational wave signal. For galaxy 3C 66B, an SMBHB candidate source, we know the sky position and redshift z to a very high precision (Hunt et al. 2021; van den Bosch et al. 2015). Because $z = 0.02 \ll 0.1$ and because we do not expect stringent constraints on D , we assume $D = D_L$ and use the linear approximation $v = cz$ for simplicity. To develop high-precision cosmology with PTAs as part of future work, it is necessary to use full expressions for D and v , while also correcting the recession velocities based on peculiar velocities of galaxies (Abbott et al. 2017b). In any case, the key requirement of a PTA in cosmology, based on targeted CW searches, is to constrain the luminosity distance of an SMBHB candidate.

Therefore, to obtain a posterior on H_0 , we place constraints on the luminosity distance D_L to 3C 66B with the PPTA DR3. We impose a prior $\pi(D_L) = \mathcal{U}(10^{-2}, 10^3) \text{ Mpc}$. We chose a prior on $\log_{10} f_{\text{GW}}$ as in Section 4.2, and we chose a prior on $\log_{10} \mathcal{M}$ as in Section 4.1. Based on the posterior on $\pi(D_L)$ and Equation 6, we obtain a posterior on H_0 in Figure 6. The values H_0 are shown along the bottom horizontal axis. The values of $\pi(D_L)$ corresponding to H_0 based on

Equation 6 and the known redshift of 3C 66B are shown along the top horizontal axis. Because we do not detect a gravitational wave signal, we rule out the nearest luminosity distances at which the SMBHB candidate is located. Our lower limits on D_L determine our upper limits on H_0 . Our choice of $\pi(D_L)$ is presented as the toy model, which is why we do not currently report the 95% credible upper-limit value for H_0 . Overall, we find that the PTA constraints on H_0 based on our targeted search for the SMBHB at 3C 66B are not competitive with those of the state-of-the-art cosmological experiments. However, a detection of CGWs from an SMBHB in the targeted search, especially with the resolved pulsar term, may prove to be useful.

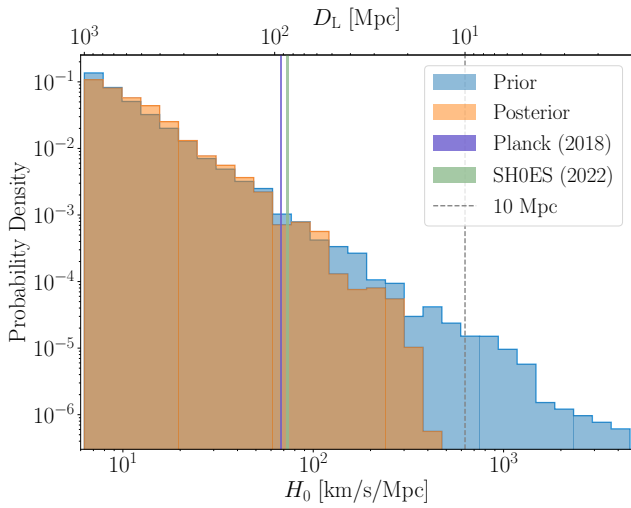


Figure 6. Posterior on the Hubble constant. The prior is shown as the blue histogram and the posterior as the orange histogram. The uncertainty regions for the Hubble constant from Planck Collaboration et al. (2020) and the SH0ES collaboration (Riess et al. 2022) are plotted as the purple and green regions, respectively. The luminosity distance of 10 Mpc is also plotted for reference as the black vertical dashed line, showing that the nearest distances from the Earth are ruled out.

5. CONCLUSION

Using the PPTA DR3, we conduct a targeted multi-messenger search for an SMBHB at the center of 3C 66B. We search for a CGW signal by performing model selec-

tion, where we compare a model with a CGW signal to the null hypothesis. With priors carefully matched to the EM model, we find a log Bayes factor of $\ln \mathcal{B} = 0.22$. This suggests we can neither confirm nor rule out the EM model. We also find frequentist $\mathcal{F}_e = 5.04$ with an associated false alarm probability of $\text{FAP} = 0.50$, which confirms non-detection of the signal. Based on the background estimation, we find that $\mathcal{F}_e = 5.04$ corresponds to the p-value $p = 0.04$, about 2.1σ .

Following non-detection, we place upper limits on the mass as $\mathcal{M} < 6.05 \times 10^8 M_\odot$ and strain amplitude $\log_{10}(h_0) < -14.44$, at 95% credibility. For both the mass and the strain, we rule out about 50% of the parameter space of the EM model. Using conservative priors, we still rule out a portion of the EM model, finding a 95% upper limit on the chirp mass of $\mathcal{M} < 9.55 \times 10^8 M_\odot$ and for the strain amplitude we find a value of $h_0 < -14.20$. Finally, we demonstrate a proof of principle that it is possible to use firmly established SMBHB candidates in targeted searches with PTAs as standard sirens, complementary to high-precision cosmology. In particular, we calculate the posterior of the luminosity distance to 3C 66B, based on which we obtain constraints on the Hubble constant.

6. ACKNOWLEDGMENTS

Murriyang, CSIRO’s Parkes radio telescope, is part of the Australia Telescope National Facility (<https://ror.org/05qajvd42>) which is funded by the Australian Government for operation as a National Facility managed by CSIRO. We acknowledge the Wiradjuri people as the Traditional Owners of the Observatory site. This research has made use of the NASA/IPAC Extragalactic Database, which is funded by the National Aeronautics and Space Administration and operated by the California Institute of Technology. Parts of this work were supported by the Australian Research Council Centre of Excellence for Gravitational Wave Astronomy (OzGrav) through grant CE230100016

Software: PTMCMCSAMPLER (Ellis & van Haasteren 2019), ENTERPRISE (Ellis et al. 2019), ENTERPRISE_WARP at github.com/bvgoncharov/enterprise_warp, ENTERPRISE_EXTENSIONS (Taylor et al. 2021).

REFERENCES

- Abbott, B. P., Abbott, R., Abbott, T. D., et al. 2017a, PhRvL, 119, 161101, doi: [10.1103/PhysRevLett.119.161101](https://doi.org/10.1103/PhysRevLett.119.161101)
- . 2017b, Nature, 551, 85, doi: [10.1038/nature24471](https://doi.org/10.1038/nature24471)
- Agarwal, N., Agazie, G., Anumalapudi, A., et al. 2025, arXiv e-prints, arXiv:2508.16534.
- <https://arxiv.org/abs/2508.16534>

- Agazie, G., Anumalapudi, A., Archibald, A. M., et al. 2023a, *ApJL*, 951, L8, doi: [10.3847/2041-8213/acdac6](https://doi.org/10.3847/2041-8213/acdac6)
- . 2023b, *ApJL*, 951, L50, doi: [10.3847/2041-8213/ace18a](https://doi.org/10.3847/2041-8213/ace18a)
- Agazie, G., Arzoumanian, Z., Baker, P. T., et al. 2024, *ApJ*, 963, 144, doi: [10.3847/1538-4357/ad1ff61](https://doi.org/10.3847/1538-4357/ad1ff61)
- Aggarwal, K., Arzoumanian, Z., Baker, P. T., et al. 2019, *ApJ*, 880, 116, doi: [10.3847/1538-4357/ab2236](https://doi.org/10.3847/1538-4357/ab2236)
- Antoniadis, J., Arzoumanian, Z., Babak, S., et al. 2022, *MNRAS*, 510, 4873, doi: [10.1093/mnras/stab3418](https://doi.org/10.1093/mnras/stab3418)
- Arzoumanian, Z., Brazier, A., Burke-Spolaor, S., et al. 2016, *ApJ*, 821, 13, doi: [10.3847/0004-637X/821/1/13](https://doi.org/10.3847/0004-637X/821/1/13)
- Arzoumanian, Z., Baker, P. T., Blumer, H., et al. 2020a, *ApJL*, 905, L34, doi: [10.3847/2041-8213/abd401](https://doi.org/10.3847/2041-8213/abd401)
- Arzoumanian, Z., Baker, P. T., Brazier, A., et al. 2020b, *ApJ*, 900, 102, doi: [10.3847/1538-4357/ababa1](https://doi.org/10.3847/1538-4357/ababa1)
- Arzoumanian, Z., Baker, P. T., Blecha, L., et al. 2023, *ApJL*, 951, L28, doi: [10.3847/2041-8213/acdbc7](https://doi.org/10.3847/2041-8213/acdbc7)
- Burke-Spolaor, S., Taylor, S. R., Charisi, M., et al. 2019, *A&A Rv*, 27, 5, doi: [10.1007/s00159-019-0115-7](https://doi.org/10.1007/s00159-019-0115-7)
- Chatterjee, S., Briskin, W. F., Vlemmings, W. H. T., et al. 2009, *ApJ*, 698, 250, doi: [10.1088/0004-637X/698/1/250](https://doi.org/10.1088/0004-637X/698/1/250)
- Chen, S., Caballero, R. N., Guo, Y. J., et al. 2021, *MNRAS*, 508, 4970, doi: [10.1093/mnras/stab2833](https://doi.org/10.1093/mnras/stab2833)
- Deller, A. T., Goss, W. M., Briskin, W. F., et al. 2019, *ApJ*, 875, 100, doi: [10.3847/1538-4357/ab11c7](https://doi.org/10.3847/1538-4357/ab11c7)
- Ding, H., Deller, A. T., Stappers, B. W., et al. 2023, *MNRAS*, 519, 4982, doi: [10.1093/mnras/stac3725](https://doi.org/10.1093/mnras/stac3725)
- Ellis, J., & Van Haasteren, R. 2017, *jellis18/PTMCMCSampler*: Official Release, 1.0.0, Zenodo, doi: [10.5281/zenodo.1037579](https://doi.org/10.5281/zenodo.1037579)
- Ellis, J., & van Haasteren, R. 2019, *PTMCMCSampler*: Parallel tempering MCMC sampler package written in Python, *Astrophysics Source Code Library*, record ascl:1912.017
- Ellis, J. A., Siemens, X., & Creighton, J. D. E. 2012, *ApJ*, 756, 175, doi: [10.1088/0004-637X/756/2/175](https://doi.org/10.1088/0004-637X/756/2/175)
- Ellis, J. A., Vallisneri, M., Taylor, S. R., & Baker, P. T. 2019, ENTERPRISE: Enhanced Numerical Toolbox Enabling a Robust Pulsar Inference Suite, *Astrophysics Source Code Library*, record ascl:1912.015
- EPTA Collaboration, InPTA Collaboration, Antoniadis, J., et al. 2023, *A&A*, 678, A50, doi: [10.1051/0004-6361/202346844](https://doi.org/10.1051/0004-6361/202346844)
- Goncharov, B., Shannon, R. M., Reardon, D. J., et al. 2021a, *ApJL*, 917, L19, doi: [10.3847/2041-8213/ac17f4](https://doi.org/10.3847/2041-8213/ac17f4)
- Goncharov, B., Reardon, D. J., Shannon, R. M., et al. 2021b, *MNRAS*, 502, 478, doi: [10.1093/mnras/staa3411](https://doi.org/10.1093/mnras/staa3411)
- Goncharov, B., Thrane, E., Shannon, R. M., et al. 2022, *ApJL*, 932, L22, doi: [10.3847/2041-8213/ac76bb](https://doi.org/10.3847/2041-8213/ac76bb)
- Goncharov, B., Sardana, S., Sesana, A., et al. 2024, arXiv e-prints, arXiv:2409.03627, doi: [10.48550/arXiv.2409.03627](https://doi.org/10.48550/arXiv.2409.03627)
- Hee, S., Handley, W. J., Hobson, M. P., & Lasenby, A. N. 2016, *MNRAS*, 455, 2461, doi: [10.1093/mnras/stv2217](https://doi.org/10.1093/mnras/stv2217)
- Hellings, R. W., & Downs, G. S. 1983, *ApJL*, 265, L39, doi: [10.1086/183954](https://doi.org/10.1086/183954)
- Hobbs, G., Manchester, R. N., Dunning, A., et al. 2020, *PASA*, 37, e012, doi: [10.1017/pasa.2020.2](https://doi.org/10.1017/pasa.2020.2)
- Hopkins, P. F., Richards, G. T., & Hernquist, L. 2007, *ApJ*, 654, 731, doi: [10.1086/509629](https://doi.org/10.1086/509629)
- Hunt, L. R., Johnson, M. C., Cigan, P. J., Gordon, D., & Spitzak, J. 2021, *AJ*, 162, 121, doi: [10.3847/1538-3881/ac135d](https://doi.org/10.3847/1538-3881/ac135d)
- Iguchi, S., Okuda, T., & Sudou, H. 2010, *ApJL*, 724, L166, doi: [10.1088/2041-8205/724/2/L166](https://doi.org/10.1088/2041-8205/724/2/L166)
- Jenet, F. A., Lommen, A., Larson, S. L., & Wen, L. 2004, *ApJ*, 606, 799, doi: [10.1086/383020](https://doi.org/10.1086/383020)
- Jennings, R. J., Kaplan, D. L., Chatterjee, S., Cordes, J. M., & Deller, A. T. 2018, *ApJ*, 864, 26, doi: [10.3847/1538-4357/aad084](https://doi.org/10.3847/1538-4357/aad084)
- Kaspi, V. M., Taylor, J. H., & Ryba, M. F. 1994, *ApJ*, 428, 713, doi: [10.1086/174280](https://doi.org/10.1086/174280)
- Lentati, L., Alexander, P., Hobson, M. P., et al. 2013, *PhRvD*, 87, 104021, doi: [10.1103/PhysRevD.87.104021](https://doi.org/10.1103/PhysRevD.87.104021)
- Moran, A., Mingarelli, C. M. F., Bedell, M., Good, D., & Spergel, D. N. 2023, *ApJ*, 954, 89, doi: [10.3847/1538-4357/acec75](https://doi.org/10.3847/1538-4357/acec75)
- Ng, C., Bailes, M., Bates, S. D., et al. 2014, *MNRAS*, 439, 1865, doi: [10.1093/mnras/stu067](https://doi.org/10.1093/mnras/stu067)
- Park, R. S., Folkner, W. M., Williams, J. G., & Boggs, D. H. 2021, *AJ*, 161, 105, doi: [10.3847/1538-3881/abd414](https://doi.org/10.3847/1538-3881/abd414)
- Petrov, P., Taylor, S. R., Charisi, M., & Ma, C.-P. 2024, *ApJ*, 976, 129, doi: [10.3847/1538-4357/ad7b14](https://doi.org/10.3847/1538-4357/ad7b14)
- Planck Collaboration, Aghanim, N., Akrami, Y., et al. 2020, *A&A*, 641, A6, doi: [10.1051/0004-6361/201833910](https://doi.org/10.1051/0004-6361/201833910)
- Reardon, D. J., Zic, A., Shannon, R. M., et al. 2023, *ApJL*, 951, L7, doi: [10.3847/2041-8213/acdd03](https://doi.org/10.3847/2041-8213/acdd03)
- Reardon, D. J., Bailes, M., Shannon, R. M., et al. 2024, *ApJL*, 971, L18, doi: [10.3847/2041-8213/ad614a](https://doi.org/10.3847/2041-8213/ad614a)
- Riess, A. G., Yuan, W., Macri, L. M., et al. 2022, *ApJL*, 934, L7, doi: [10.3847/2041-8213/ac5c5b](https://doi.org/10.3847/2041-8213/ac5c5b)
- Romano, J. D., & Cornish, N. J. 2017, *Living Reviews in Relativity*, 20, 2, doi: [10.1007/s41114-017-0004-1](https://doi.org/10.1007/s41114-017-0004-1)
- Schutz, B. F. 1986, *Nature*, 323, 310, doi: [10.1038/323310a0](https://doi.org/10.1038/323310a0)
- Shklovskii, I. S. 1970, *Soviet Ast.*, 13, 562
- Sudou, H., Iguchi, S., Murata, Y., & Taniguchi, Y. 2003, *Science*, 300, 1263, doi: [10.1126/science.1082817](https://doi.org/10.1126/science.1082817)

- Taylor, S. R., Baker, P. T., Hazboun, J. S., Simon, J., & Vigeland, S. J. 2021, *enterprise_extensions*.
https://github.com/nanograv/enterprise_extensions
- Taylor, S. R., Huerta, E. A., Gair, J. R., & McWilliams, S. T. 2016, *ApJ*, 817, 70,
doi: [10.3847/0004-637X/817/1/70](https://doi.org/10.3847/0004-637X/817/1/70)
- Truant, R. J., Izquierdo-Villalba, D., Sesana, A., et al. 2025, arXiv e-prints, arXiv:2504.01074,
doi: [10.48550/arXiv.2504.01074](https://doi.org/10.48550/arXiv.2504.01074)
- van den Bosch, R. C. E., Gebhardt, K., Gültekin, K., Yıldırım, A., & Walsh, J. L. 2015, *ApJS*, 218, 10,
doi: [10.1088/0067-0049/218/1/10](https://doi.org/10.1088/0067-0049/218/1/10)
- van Haasteren, R., Levin, Y., McDonald, P., & Lu, T. 2009, *MNRAS*, 395, 1005,
doi: [10.1111/j.1365-2966.2009.14590.x](https://doi.org/10.1111/j.1365-2966.2009.14590.x)
- Verbiest, J. P. W., Bailes, M., Coles, W. A., et al. 2009, *MNRAS*, 400, 951, doi: [10.1111/j.1365-2966.2009.15508.x](https://doi.org/10.1111/j.1365-2966.2009.15508.x)
- Yao, J. M., Manchester, R. N., & Wang, N. 2017, *ApJ*, 835, 29, doi: [10.3847/1538-4357/835/1/29](https://doi.org/10.3847/1538-4357/835/1/29)
- Zhao, S.-Y., Chen, Z.-C., Cardinal Tremblay, J., et al. 2025, arXiv e-prints, arXiv:2508.13944,
doi: [10.48550/arXiv.2508.13944](https://doi.org/10.48550/arXiv.2508.13944)
- Zhu, X.-J., Cui, W., & Thrane, E. 2019, *MNRAS*, 482, 2588, doi: [10.1093/mnras/sty2849](https://doi.org/10.1093/mnras/sty2849)
- Zhu, X. J., Wen, L., Xiong, J., et al. 2016, *MNRAS*, 461, 1317, doi: [10.1093/mnras/stw1446](https://doi.org/10.1093/mnras/stw1446)
- Zic, A., Reardon, D. J., Kapur, A., et al. 2023, *PASA*, 40, e049, doi: [10.1017/pasa.2023.36](https://doi.org/10.1017/pasa.2023.36)

APPENDIX

A. A CONTINUOUS GRAVITATIONAL WAVE FROM AN SMBHB

Let us start by considering a plane wave traveling from an SMBHB to the Solar System barycenter (SSB) to which pulse arrival times are referenced. A unit vector that points from the CGW source to the SSB is

$$\hat{\Omega} = (\phi, \theta) = -\sin\theta\cos\phi\hat{x} - \sin\theta\sin\phi\hat{y} - \cos\theta\hat{z}, \quad (\text{A1})$$

where $(\hat{x}, \hat{y}, \hat{z})$ is the Cartesian coordinate basis with the North Celestial Pole in the \hat{z} direction, and the Vernal Equinox is in the \hat{x} direction. A polar angle θ and an azimuthal angle ϕ of the source are related to the equatorial coordinate right ascension R.A. = ϕ and declination Dec. = $\pi/2 - \theta$.

The wave is characterized by the metric strain rank-2 tensor in the transverse traceless gauge, indexed with (a, b) ,

$$h_{ab}(t, \hat{\Omega}) = e_{ab}^+(\hat{\Omega}) h_+(t, \hat{\Omega}) + e_{ab}^\times(\hat{\Omega}) h_\times(t, \hat{\Omega}). \quad (\text{A2})$$

Components $h_{+,\times}$ are the polarization amplitudes, and $e_{ab}^{+,\times}$ are the polarization tensors. Rotating the Cartesian coordinate system such that it is oriented towards a CGW source, we obtain new basis vectors in $(\hat{x}, \hat{y}, \hat{z})$ as in [Arzoumanian et al. \(2023\)](#):

$$\begin{aligned} \hat{n} &= (\sin\theta\cos\phi, \sin\theta\sin\phi, \cos\theta) = -\hat{\Omega}, \\ \hat{p} &= (\cos\psi\cos\theta\cos\phi - \sin\psi\sin\phi, \\ &\quad \cos\psi\cos\theta\sin\phi + \sin\psi\cos\phi, -\cos\psi\sin\theta), \\ \hat{q} &= (\sin\psi\cos\theta\cos\phi + \cos\psi\sin\phi, \\ &\quad \sin\psi\cos\theta\sin\phi - \cos\psi\cos\phi, -\sin\psi\sin\theta). \end{aligned} \quad (\text{A3})$$

Polarization angle ψ is the angle between the natural polarization basis (at source) and the reference polarization basis (at SSB). With this, polarization tensors are expressed as

$$\begin{aligned} e_{ab}^+ &= \hat{p}_a \hat{p}_b - \hat{q}_a \hat{q}_b, \\ e_{ab}^\times &= \hat{p}_a \hat{q}_b + \hat{q}_a \hat{p}_b. \end{aligned} \quad (\text{A4})$$

The response of a PTA to the plane wave is described by the antenna pattern function ([Romano & Cornish 2017](#))

$$F^A(\hat{\Omega}) \equiv \frac{1}{2} \frac{\hat{u}^a \hat{u}^b}{1 + \hat{\Omega} \cdot \hat{u}} e_{ab}^A(\hat{\Omega}), \quad (\text{A5})$$

where \hat{u} is the unit vector pointing from the SSB to the pulsar. This function describes a pulsar's geometrical sensitivity to the CGW source ([Taylor et al. 2016](#)). Pulsar timing delays δt are then expressed as

$$\delta t(t, \hat{\Omega}) = F^+(\hat{\Omega}) \delta t'_+(t) + F^\times(\hat{\Omega}) \delta t'_\times(t), \quad (\text{A6})$$

where we implied that $\delta t_{+,\times}$ is the time integral of $h_{+,\times}$, and $\delta t'_{+,\times}$ is the difference between the delay experienced at the SSB (Earth) and the signal induced at the pulsar. This difference is

$$\delta t'_{+,\times}(t) = \delta t_{+,\times}(t_p) - \delta t_{+,\times}(t), \quad (\text{A7})$$

where t is the time when the CGW passes the SSB and t_p is the time when the CGW passes the pulsar. One can then geometrically relate t and t_p ,

$$t_p = t - \frac{L}{c} (1 + \hat{\Omega} \cdot \hat{u}), \quad (\text{A8})$$

where L as the distance to the pulsar.

For an SMBHB, at zeroth post-Newtonian order, we arrive at our model of the CGW projected onto a PTA detector,

$$\begin{aligned} \delta t'_+(t) &= \frac{(GM)^{5/3}}{D_L c^4 \omega(t)^{1/3}} [-\sin 2\Phi(t)(1 + \cos^2 \iota)], \\ \delta t'_\times(t) &= \frac{(GM)^{5/3}}{D_L c^4 \omega(t)^{1/3}} [2 \cos 2\Phi(t) \cos \iota], \end{aligned} \quad (\text{A9})$$

where ι is the SMBHB inclination angle, D_L is the luminosity distance, $\omega(t) = \pi f_{\text{GW}}$ is the angular orbital frequency², $\Phi(t)$ is the phase,

$$\mathcal{M} \equiv \frac{(m_1 m_2)^{3/5}}{(m_1 + m_2)^{1/5}} \quad (\text{A10})$$

is the chirp mass, $m_{1,2}$ are SMBHB component masses. The last observation in the PPTA dataset (March 8, 2022, or MJD 59646) is used as a reference time. The orbital phase and frequency of the SMBHB are then defined as,

$$\begin{aligned} \Phi(t) &= \Phi_0 + \frac{1}{32} \left(\frac{G\mathcal{M}}{c^3} \right)^{-5/3} [\omega_0^{-5/3} - \omega(t)^{-5/3}], \\ \omega(t) &= \omega_0 \left(1 - \frac{256}{5} \left(\frac{G\mathcal{M}}{c^3} \right)^{5/3} \omega_0^{8/3} t \right)^{-3/8}, \end{aligned} \quad (\text{A11})$$

with Φ_0 being the initial orbital phase and ω_0 the initial orbital frequency, one may notice that it is equivalent to Equation 3.

Chirp mass and frequency are redshifted for CGW sources at cosmological distances, such that the observed “o” values are related to intrinsic source “s” values as

$$\begin{aligned} \mathcal{M}_o &= \mathcal{M}_s(1+z), \\ f_o &= \frac{f_s}{1+z}. \end{aligned} \quad (\text{A12})$$

For 3C 66B, $z = 0.02 \ll 1$, so given our measurement uncertainty we assume $\mathcal{M} = \mathcal{M}_o = \mathcal{M}_s$ and $f = f_o = f_s$.

B. ANALYSIS OF THE 3-MM DATA

Although key details of the analysis of the 3-mm data are provided in [Iguchi et al. \(2010\)](#), here we provide explicit equations that we used in our reanalysis. Throughout, we switch between the velocity v and the boost parameter $\beta = v/c$, which may also have subscripts “bl,0” and “app” for the absolute binary component velocity around the center of gravity and the apparent relativistic jet velocity, respectively. First, we point out that Equations 1 and 2 from [Iguchi et al. \(2010\)](#) can be expressed directly in terms of (β, ι) ,

$$\begin{cases} \beta = \sqrt{(1-r)^2 + (\beta_{\text{app}} r)^2}, \\ \iota = \text{atan2}(\beta_{\text{app}} r, 1-r), \end{cases} \quad (\text{B13})$$

where r is the ratio

$$r = \frac{P_{\text{obs}}}{(1+z)P_k}. \quad (\text{B14})$$

Next, (β, ι) are required in the calculation of the absolute value of the rotational velocity of one of the binary components, which has a jet, around the center of mass. This velocity causes a Doppler boosting of the flux. We solve Equation 4 from [Iguchi et al. \(2010\)](#) for this velocity, obtaining

$$\beta_{\text{bl},0} = \frac{1 - \beta \cos \iota}{\sin \iota} \frac{S_r^{\frac{1}{3+\alpha}} - 1}{S_r^{\frac{1}{3+\alpha}} + 1}. \quad (\text{B15})$$

Considering a Keplerian motion in a circular orbit, we use the following expressions of the orbital radius R and the orbital separation a ,

$$\begin{cases} a = \sqrt[3]{\frac{GM_{\text{tot}}P_k^2}{(2\pi)^2}}, \\ R = \frac{v_{\text{bl},0}P_k}{2\pi}. \end{cases} \quad (\text{B16})$$

Introducing $x \equiv R/a$, one finds that $x = m/M_{\text{tot}}$ with m the mass of a lighter black hole for the case where a heavier black hole emits a jet (smaller radius). Similarly, one finds $x = M/M_{\text{tot}}$ with M the mass of a heavier black hole for the case where a lighter black hole emits a jet (larger radius). Apparently, for the calculation of the chirp mass, these two cases reduce to the same answer due to a symmetry in $x(1-x)$ in the final expression

$$\begin{cases} \mathcal{M} = M_{\text{tot}}[x(1-x)]^{3/5}, \\ x \equiv \frac{R}{a} = v_{\text{bl},0} \sqrt[3]{\frac{P_k}{2\pi GM_{\text{tot}}}}. \end{cases} \quad (\text{B17})$$

² The SMBHB angular orbital frequency is half the CGW angular frequency $2\pi f_{\text{GW}}$.

C. PULSAR DISTANCES

Pulsar distances are required in the calculation of the expected signal when modeling the pulsar term of the CGW signal. Pulsar distances are measured using very-long-baseline-interferometry (VLBI) astrometry, optical astrometry, timing, and the [Shklovskii \(1970\)](#) effect. A list of the priors used for each pulsar, as well as the technique used to find this distance, is listed in Table 2. We impose a Gaussian prior on pulsar distance in accordance with the estimates found in the literature. When no such estimates are available for a given pulsar, we impose a sufficiently conservative prior $\mathcal{N}(1000, 200)$ [pc]. Distance estimates based on pulsar dispersion measure are not used due to the large uncertainties in the electron density model ([Yao et al. 2017](#)).

PSR	Distance [pc]	Measurement	Reference
J0030+0451	329^{+6}_{-5}	VLBI astrometry	Ding et al. (2023)
J0125-2327	1000 ± 200	-	Ellis & Van Haasteren (2017)
J0437-4715	156.96 ± 0.11	Shklovskii effect	Shklovskii (1970); Reardon et al. (2024)
J0613-0200	125 ± 54.69	Timing	Verbiest et al. (2009)
J0614-3329	1000 ± 200	-	Ellis & Van Haasteren (2017)
J0711-6830	1000 ± 200	-	Ellis & Van Haasteren (2017)
J0900-3144	1000 ± 200	-	Ellis & Van Haasteren (2017)
J1017-7156	256.41 ± 78.90	Timing	Ng et al. (2014)
J1022+1001	$720.98^{+21.31}_{-14.55}$	VLBI astrometry	Deller et al. (2019)
J1024-0719	1072^{+67}_{-49}	Optical astrometry	Moran et al. (2023)
J1045-4509	303.03 ± 174.47	Timing	Verbiest et al. (2009)
J1125-6014	1000 ± 200	-	Ellis & Van Haasteren (2017)
J1446-4701	1000 ± 200	-	Ellis & Van Haasteren (2017)
J1545-4550	1000 ± 200	-	Ellis & Van Haasteren (2017)
J1600-3053	5000 ± 3750	Timing	Verbiest et al. (2009)
J1603-7202	1000 ± 200	-	Ellis & Van Haasteren (2017)
J1643-1224	$4763.36^{+99.06}_{-104.89}$	VLBI astrometry	Ding et al. (2023)
J1713+0747	$1052.63^{+66.48}_{-55.40}$	VLBI astrometry	Chatterjee et al. (2009)
J1730-2304	510^{+30}_{-30}	VLBI astrometry	Ding et al. (2023)
J1744-1134	416.67 ± 17.36	Timing	Verbiest et al. (2009)
J1824-2452A	10000 ± 50000	VLBI astrometry	Ding et al. (2023)
J1832-0836	1000 ± 200	-	Ellis & Van Haasteren (2017)
J1857+0943	909.09 ± 165.29	VLBI astrometry	Verbiest et al. (2009)
J1902-5105	1000 ± 200	-	Ellis & Van Haasteren (2017)
J1909-3744	1265.82 ± 32.05	Timing	Verbiest et al. (2009)
J1933-6211	1000 ± 200	-	Ellis & Van Haasteren (2017)
J1939+2134	$2604.17^{+325.52}_{-311.96}$	VLBI astrometry	Ding et al. (2023)
J2124-3358	322.58 ± 57.23	Timing	Verbiest et al. (2009)
J2129-5721	2358.49 ± 489.50	Optical astrometry	Jennings et al. (2018)
J2145-0750	$623.83^{+24.51}_{-3.50}$	VLBI astrometry	Deller et al. (2019)
J2241-5236	1000 ± 200	-	Ellis & Van Haasteren (2017)

Table 2. Table describing the pulsar distances, the methods used to obtain them and the source from which they were obtained. If no distance was available, the method is listed as “-”.